PAPER

Thermal behavior in the magnetic phase diagram of the easy axis antiferromagnet $Cs_2FeCl_5 \cdot H_2O$

To cite this article: R S Freitas *et al* 2016 *J. Phys.: Condens. Matter* **28** 126007

IOP Publishing Journal of Physics: Condensed Matter
J. Phys.: Condens. Matter **28** (2016) 126007 (10pp) doi:10.1088/0953-8984/28/12/126007

Thermal behavior in the magnetic phase diagram of the easy axis antiferromagnet $Cs_2FeCl_5{\cdot}H_2O$

R S Freitas, A Paduan-Filho and C C Becerra

Instituto de Física Universidade de São Paulo CP 66318, 05314-970 São Paulo, SP, Brazil

E-mail: freitas@if.usp.br

Received 8 September 2015, revised 14 December 2015
Accepted for publication 23 December 2015
Published 2 March 2016

Abstract

The specific heat at a constant applied field $C_H(T)$ and at fixed temperatures $C_T(H)$ of single crystals of the low anisotropy antiferromagnet $Cs_2FeCl_5{\cdot}H_2O$ was measured across the different boundaries of its magnetic phase diagram, in magnetic fields up to 9 T applied parallel and perpendicular to the easy axis direction and to temperatures down to 0.3 K. The specific heat data indicate that the critical behavior along the antiferromagnetic to paramagnetic phase boundary and the spin-flop to paramagnetic phase boundary, are basically the same. We also measured the specific heat when the first order antiferromagnetic to spin-flop phase boundary is crossed at a fixed temperature. The entropy of the different magnetic phases is discussed.

Keywords: antiferromagnetic materials, phase transitions, magnetic entropy

(Some figures may appear in colour only in the online journal)

I. Introduction

Despite a recently fast increase in the discovery of a number of compounds covering a wide range of magnetic behavior, there is still a lack of experimental thermodynamic data analyzing the magnetic and calorimetric properties across the different phase transitions and its dependence on the crystal orientation with regard to the applied magnetic field direction. The family of antiferromagnets $A_2FeCl_5{\cdot}H_2O$ (A = K, Rb, Cs) for example, show long range ordering temperatures ranging from 6.6 K (Cs) to 14 K (K) [1]. Although the thermal properties of some members of this family have been previously explored at zero applied field in powder samples, the thermal properties were never investigated when a magnetic field is applied along the different crystal axes. These systems have been referred and compared to the low anisotropy classical antiferromagnet MnF_2 (T_N ~ 63.7 K) [2]. A complete phase diagram including the phase boundaries to the paramagnetic phase at low temperatures was only recently reported [3] for $Cs_2FeCl_5{\cdot}H_2O$. This sample has a slightly lower anisotropy than MnF_2 and despite its orthorhombic structure, instead of the tetragonal one observed in MnF_2, as stressed in [3] their phase diagram matches closely in a reduced temperature-field scale. When compared to MnF_2, the compound $Cs_2FeCl_5{\cdot}H_2O$ has a more favorable magnetic field scale, easily attainable using superconducting magnets, which makes it more suitable to explore the behavior of the specific heat and the magnetic entropy in the different phases and along the boundaries separating the ordered states. This study is the main purpose of this paper.

Previous magnetic studies in this low anisotropy system were carried out using powder samples focusing on the low field region of the phase diagram ($H < 2$ T) [1] and on the specific heat properties at $H = 0$ in the interval $1.5\,\text{K} < T < 30\,\text{K}$ [4]. From these works, that stand as the basic reference on the magnetic and thermal behavior on $Cs_2FeCl_5{\cdot}H_2O$, the Néel temperature found is (6.57 ± 0.05) K [1] and (6.54 ± 0.02) K [4]. An anisotropy field $H_A = 0.088$ T and an exchange field $H_E = 7.59$ T with a ratio $\alpha = H_A/H_E = 1.2 \times 10^{-2}$ were obtained from the value of the susceptibility and from the extrapolated value of the antiferromagnetic to the spin-flop critical field ($H_{AF-SF} = 1.15$ T) as the temperature goes to zero [1].This system behaves closely to a 3D system with competing antiferromagnetic interactions [1, 2]. The Cs derivative

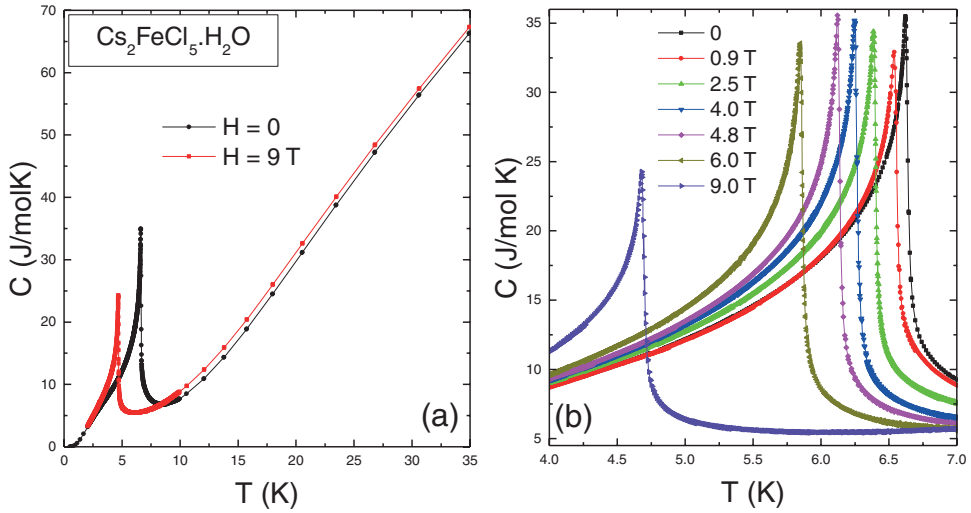

Figure 1. (a) Specific heat of $CsFeCl_5{\cdot}2H_2O$ for various magnetic fields applied along the easy axis. (a) Full temperature range up to $T = 35$ K. The lattice contribution is dominant above $T = 15$ K. (b) Detailed region around the transition to the ordered phase. Note that along an isotherm C increases with H in the ordered region.

has a distinct space groups than the other members of this family, but with similar exchange paths provided through the O–Cl and Cl–Cl bridges.

The structural characteristics of this compound is discussed in [1, 2, 5] and we refer to them for further information. The system belongs to the orthorhombic space group *Cmcm* with four molecules per unit cell. Each iron ion is surrounded by an octahedron formed by the five chlorine ions and the H_2O molecule in an apical position. The Cs ions are located in interstitial sites between the [Fe–Cl_5–H_2O] octahedrons. According to [1, 4], the principal (J_1) exchange paths between the iron ions are provided by oxygen-chlorine double bridges (Fe–Cl–H–O(H)–Fe) forming a zig–zag chain running along the c axis. Along the a direction and also within the ac planes the Fe ions are connected by [Fe–Cl–Cl–Fe] bridges with exchange paths J_2 and J_3 of the same order of magnitude but with ($J_1 \gg J_2 \sim J_3$). A comparative examination of the crystallographic and magnetic structure is provided in [6] using neutron diffraction experiments for the potassium compound of this same family, namely $K_2FeCl_5{\cdot}H_2O$ of *Pnma* space group. This study disclosed very similar exchange paths between the iron sites. Moreover the neutron study in [6] provides a careful determination of the magnetic structure of this K derivative estimating five different exchange constants all with the same sign with a hierarchical range that results in an antiferromagnetic arrangement. We assume that probably a similar magnetic structure occurs in the Cs derivative where the easy and intermediate axis are respectively along directions a and c. The systematic comparative study of [1] for this series of compounds concludes that the Cs derivative is the closest approach to a Heisenberg type antiferromagnet.

II. Experiment

Single-crystal samples of $Cs_2FeCl_5{\cdot}H_2O$ were grown at room temperature from aqueous solution with a stoichiometric ratio of $FeCl_3{\cdot}6H_2O$ and CsCl by a slow controlled evaporation of the solvent. After a growth period of two weeks, red single crystals with dimensions up to about 20 mm and well developed morphological faces were obtained. Using the morphological faces as reference planes, oriented samples with the long face parallel and perpendicular to the easy magnetic axis were prepared. The magnetization at low fields was measured with a magnetic property measurement (SQUID) system. The specific heat data were obtained using a Quantum Design Dynacool system using a standard semi-adiabatic heat pulse technique under magnetic fields up to 9 T and temperatures down to 0.3 K. The addendum heat capacity was measured separately and subtracted. In order to correctly capture the strong variation of the specific heat with temperature close to the phase transition, we used a high-resolution slope analysis of the relaxation curve of the sample's temperature during the heat pulse [7] Measurements of the specific heat as a function of the applied magnetic field in a nearly constant temperature were obtained using very small heat pulses resulting in a temperature change of the sample of less than 0.04 K during the measurements.

The sample was oriented with its easy a or the b axis parallel to the applied field. The possible miss-orientation is very small, since as we will show below, the bi-critical point in the phase diagram can be clearly identified.

II.A. Specific heat at constant applied field

The temperature dependence of the specific heat measured for different values of the external field applied along the easy a axis is plotted in figures 1(a) and (b). The low temperature region close to the paramagnetic to the ordered phase is shown in detail for different magnetic fields in figure 1(b). The lambda anomalies observed in the specific heat curves at $H = 0$ correspond to the second order transition from the paramagnetic (P) to the antiferromagnetic phase (AF). Above $H = 1.45$ T the second order anomaly mark the transition from the P state to the spin-flop (SF) phase. Therefore we can define a bicritical point (BCP) at $H_{BC} = 1.47$ T and $T_{BC} = 6.40$ K,

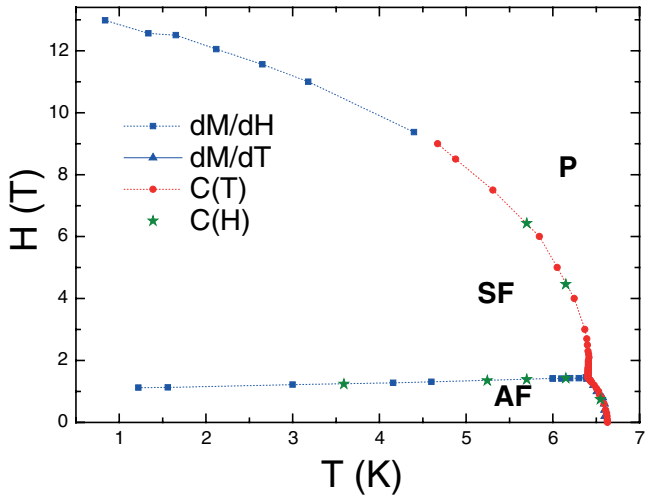

Figure 2. The magnetic phase diagram measured for the magnetic field applied along the easy *a* axis. Transitions to the P phase are second order and the boundary between the AF and SF is a line of first order transitions.

where the tree phases coexist. Those transitions are plotted in the phase diagram shown in figure 2. This figure shows transition data points obtained from magnetization and susceptibility measurements in [3] for magnetic fields up to 14 T applied along the easy axis. We will analyze these data in the next section; however a very subtle detail in the curve measured at 1.25 T is worth mentioning. This point is the subject of figure 3(a), where the specific heat (right hand scale) is compared to the corresponding AC magnetic susceptibility both measured at the same field of 1.25 T. This figure put in evidence the entrance of the system from the AF to the SF phase by crossing the AF–SF boundary when sweeping the temperature. In the specific heat this entrance is barely seen as a small bump in the data around 3.6 K, but sharply visible in the AC data as a conspicuous peak characteristic of a first order transition and also in the magnetization as the sudden rise towards the value expected when the magnetic moments are perpendicular to the applied field in the SF phase as can be seen in figure 3(a) of [3]. In the curves measured under H_{BC} the two transitions from the P to the AF phase and the first order transition from the AF to the SF phase are clearly visible as a sequence of two anomalies, the first corresponds to the second order transition to the AF phase and the smaller one to the entrance into the SF phase though a first order transition. In the figure 3(b) the specific heat is also compared for the same applied field when it is applied along and perpendicular to the easy axis. For the transverse field configuration below $T_N(H)$, the system is always in the AF phase. The comparison of the entropy related to these curves and that amount to the entropy difference between these field configurations and phases will be addressed in section III.D.

II.B. Magnetic field dependence of the specific heat along the isotherms

Figure 4 shows the behavior of the specific heat along the isotherms, as a function of the field applied parallel (figure 4(a)) and along both directions, parallel and perpendicular to the easy axis, in figure 4(b). In the paramagnetic phase we observe a gradual decrease of the specific heat as the magnetic field increases. At $T = 6.55$ K, the AF–P boundary is crosses isothermally and the lambda anomaly mark the transition from the AF to the P phase. The two other isotherms at 6.15 K and 5.7 K are below the BCP temperature and therefore two anomalies correspondent to the first order AF–SF and the second order SF–P transitions are clearly visible. The jump in the specific heat marks the first order transition and the strong lambda peak the second order transition. The isothermal traces in figure 4(b) compare, at the same temperature the behavior of the specific heat when the field is parallel and perpendicular to the easy axis. The increase of $C(H)$ along the isotherms is expected as we can observe in figure 1(b) when we move isothermally in the set of curves of increasing the applied fields. Two points are worth to mention in relation to the behavior of the isothermal $C(H)$ depicted in figure 4. The specific heat always increase with H up to the transition to the P phase when the field is perpendicular to the spin configuration, either in the SF region or in AF region. Second in the AF phase for the field along the easy axis, the specific heat decrease initially and start to increase when H approach the first order SF line. We will discuss this point in the next section.

When the AF–SF phase boundary is crossed sweeping the field at the first order transition a jump in the specific heat and on the AC susceptibility is present as shown in figure 5 measured at $T = 3.55$ K. The increase in the value of C is associated with the latent heat that accompanies this first order transition and to our knowledge this is the first comparison of these two thermodynamic parameters when such phase boundary is crossed. The increase in the value of the specific heat across the transition is accompanied by an increase in the value of the magnetic susceptibility and a jump in the magnetization ($\Delta\chi H$).

III. Analysis and discussion

III.A. Magnetic specific heat

The specific heat measured at $H = 0$ and 9 T are shown in figure 1(a). Although it is expected that the lattice contribution C_{latt} remains the same at high magnetic fields, our data indicate a higher value of the C_{latt} measured under 9 T pointing to a possible magneto-elastic contribution in the paramagnetic phase. In the following discussion we assume that close to the ordered phases the lattice contribution is basically the same for all applied fields, and we will subtract the same C_{latt} ($H = 0$) to obtain the magnetic contribution to the entropy. Since all the $C_m(H)$ curves seems to converge in the region below 1.5 K we will also extend the same asymptotic behavior of the $H = 0$ curve to the other fields. The specific heat at zero applied field from 0.3 K to 30 K is shown in figure 6. Our data are in very good agreement with the previously reported in [4], with the difference within 1%. However our results are extended to much lower temperatures going down to $T = 0.3$ K. The Debye lattice contribution to

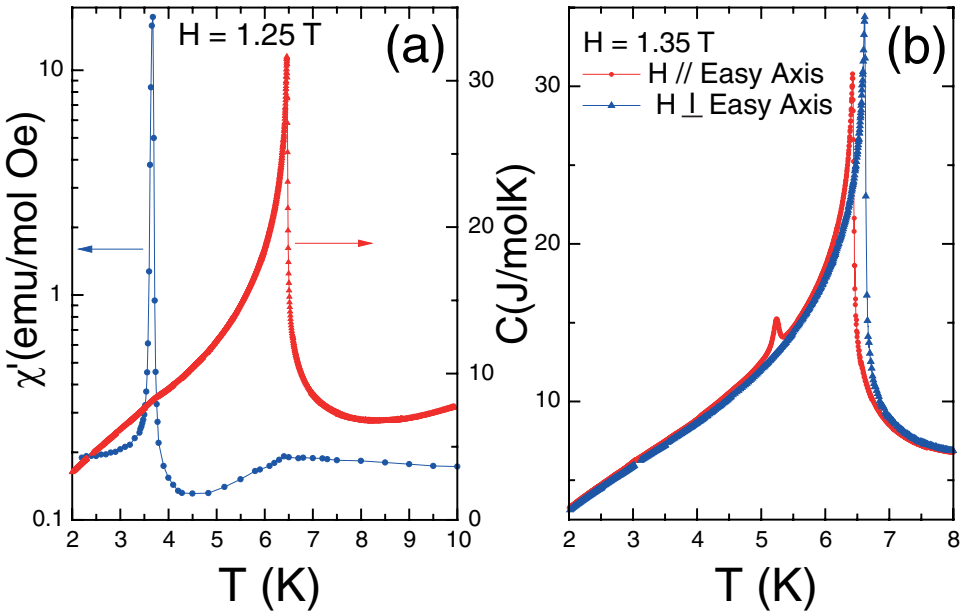

Figure 3. (a) Temperature dependence of the real part of the susceptibility and specific heat measured at the same field (1.25 T) applied along the easy axis. (b) Specific heat as a function of temperature at a slightly higher field $H = 1.35$ T applied parallel and perpendicular to the easy axis. The second order transition P–AF and first order transition AF–SF are evident.

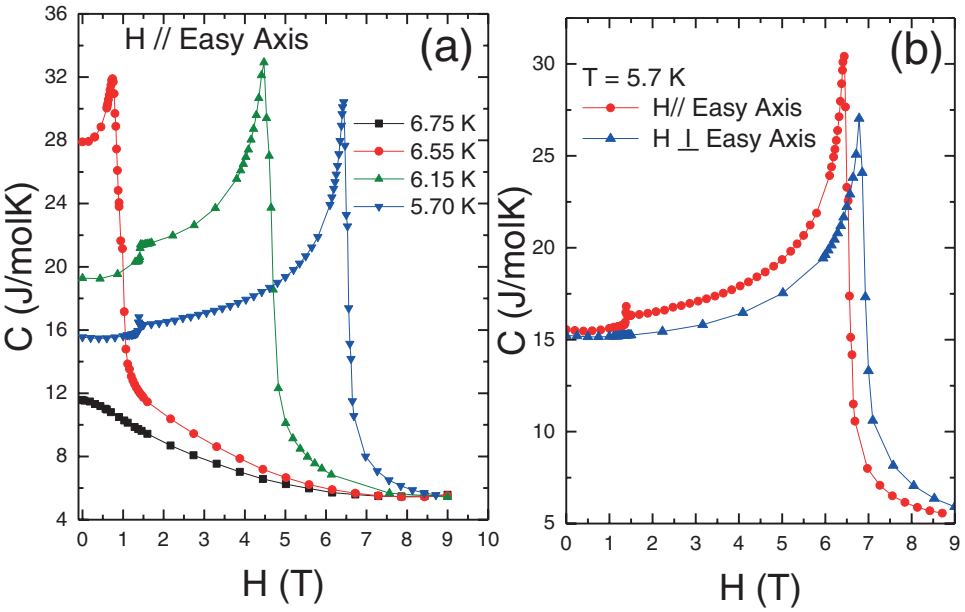

Figure 4. Isothermal scans of the specific heat at different temperatures (a) and field configuration (b). The transition (T, H) points are marked by a star symbol in the phase diagram of figure 2.

the specific heat was obtained using the same procedure outlined in [4], which is based on a fit of the high temperature part of the measured specific heat to an asymptotically convergent series of odd powers of the temperature. The resulting curve is shown in figure 6 which has a leading Debye contribution. The magnetic contribution to the specific heat C_m/R is obtained after the subtraction of this lattice contribution as shown in figure 6 for $H = 0$ and in figure 10 for different values of the applied magnetic field. The area below the curve C_m/T between 0.3 and 30 K gives a total entropy gain of ≈1.8 (see figure 10), in good agreement with the theoretically expected $\Delta S/R = \ln(2S + 1) = 1.79$ for the magnetic ion Fe^{+3} with $S = 5/2$.

III.B. Free spin wave contribution to the specific heat at low temperatures

For an isotropic antiferromagnet with no anisotropy at zero applied field, the spin wave theory developed by Kubo [8] and Eisele and Keffer [9] predicts that the specific heat at low temperatures follows a T^3 law. In the figure 7 the data for $H = 0$ of C_m/T versus T^2 is plotted. The expected anti-ferromagnetic

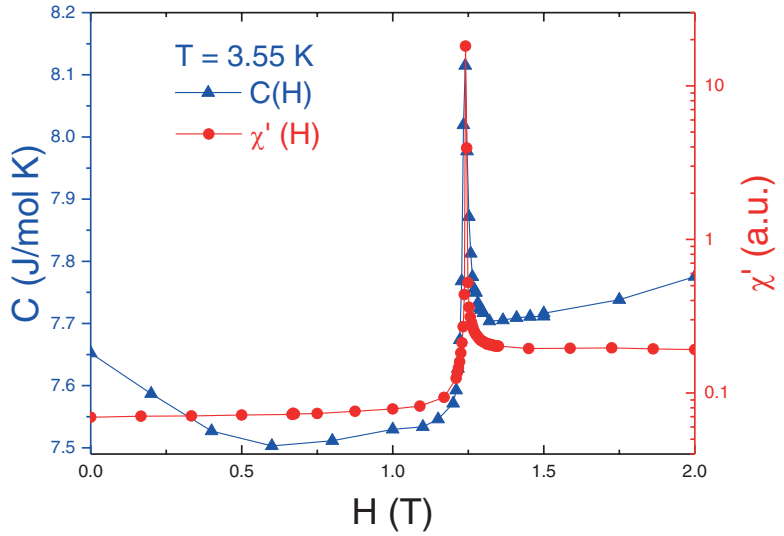

Figure 5. Specific heat and the real part of the susceptibility isothermal at the spin-flop transition.

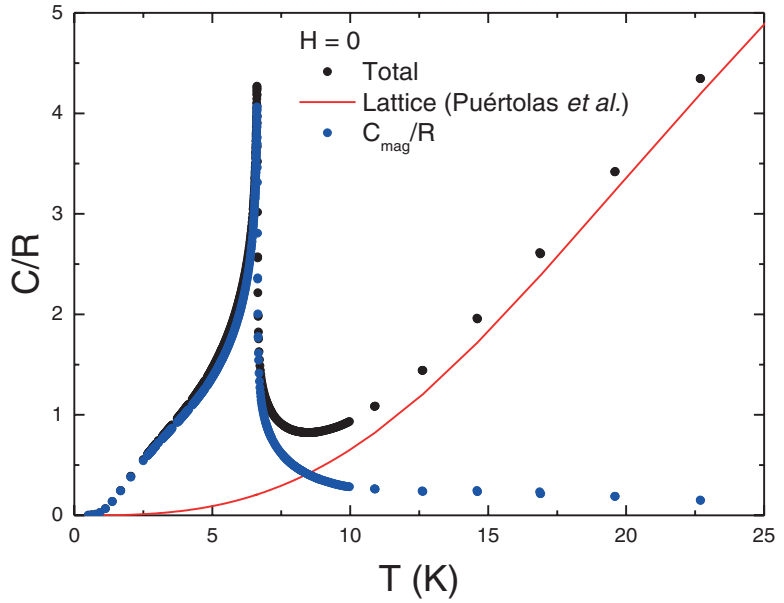

Figure 6. Lattice and magnetic contributions to the specific heat. The solid curve is the Debye contribution to the total specific heat. This solid line is drawn using the coefficient given in [4] for the lattice heat capacity.

behavior predicted by Kubo is restricted to temperatures in the range $3.7 < T < 5.2$ K. In the high temperature side the effect of the critical fluctuations associated with the AF transition anomaly dominates and in the low side a strong suppression of the T^3 law is evident. The theoretical low temperature predictions for the magnetic heat capacity at zero field when a finite anisotropy is considered was worked out by Eisele and Keffer [9] and for applied fields below the spin-flop field transition by Joenk [10]. At low temperatures an exponential suppression of C_m due to the introduction of an energy gap induced by the anisotropy in free spin-wave excitation spectrum occurs. A detailed discussion can be found in the above referred papers and also in [11]. Our experimental data shown in the inset of figure 7 depicts clearly that at low temperatures the influence of such an energy gap is present.

For anisotropic antiferromagnets [9–11] and a magnetic field H applied along the easy axis the free spin wave theory gives a heat capacity

$$C_{\mathrm{H}}(H,T) = A\left(\frac{T}{T_{\mathrm{E}}}\right)^3 C(H, t_{\mathrm{AE}}),$$

where A is a structure dependent constant. For a simple cubic structure ($Z = 6$) the analytic expression for $C = C(H, t_{\mathrm{AE}})$ is given by Joenk [10], $T_{\mathrm{E}} = 3T_{\mathrm{N}}/(S+1)$ and $t_{\mathrm{AE}} = T/T_{\mathrm{AE}}$ in a reduced temperature that encodes the anisotropy of the system. T_{AE} is a measure of the anisotropic exchange gap and is related to the transition spin-flop field $H_{\mathrm{SF}} = (\sqrt{2H_{\mathrm{A}}H_{\mathrm{E}} + H_{\mathrm{A}}^2})$ at $T \to 0$ as

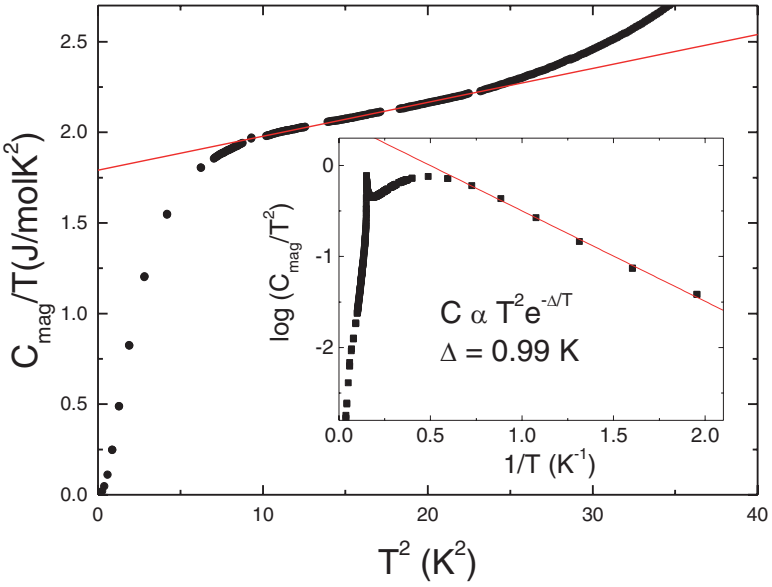

Figure 7. Magnetic specific heat at zero magnetic field plotted as $C_{\rm mag}/T$ versus T^2. The inset shows the expected gap induced by anisotropy at low temperatures.

$$T_{\rm AE} = \frac{\hbar\mu_{\rm B}}{k_{\rm B}}\left(\sqrt{2H_{\rm A}}H_{\rm E} + H_{\rm A}^2\right) \cong T_{\rm E}\sqrt{2\alpha}$$

The last approximation is valid for $H_{\rm A} \ll H_{\rm E}$, $\alpha = H_{\rm A}/H_{\rm E}$ being the ratio of the exchange and anisotropy fields.

We will consider the case of zero applied field since our data, in this case, extends to 0.5 K. The effect of the anisotropy at temperatures below $T_{\rm AE}$ is to introduce a gap that suppresses the T^3 behavior exponentially as suggested by the data in figure 7. In fact since this system has an orthorhombic symmetry two energy gaps are expected as shown by Campo *et al* [6] for compounds of the same family. From our phase diagram only one of these gaps are measured related to the anisotropy between the easy and intermediate axis. Using the experimentally measured critical fields in the limit of $T \to 0$ [3] namely: $H_{\rm sf} = 1.15$ T; $\alpha = H_{\rm A}/H_{\rm E} = 1.4 \times 10^{-2}$; $H_{\rm E} = 7.59$ T; $T_{\rm N} = 6.6$ K and with $S = 5/2$ we obtain from these values with $H_{\rm SF} = H_{\rm E}\sqrt{2\alpha}$, an exchange temperature $T_{\rm E} = (1/3)(S+1)T_{\rm N} \to T_{\rm E} = (6/7)T_{\rm N} = 5.62$ K and a anisotropy gap temperature $T_{\rm AE} \cong T_{\rm E}\sqrt{2\alpha} = 0.94$ K.

The insertion of these values in the expressions given in [9] and [10] leads to a suppression in the specific heat at low temperatures $T < T_{\rm AE}$ that is much slower than the experimentally measured. It is worth noting that in an orthorhombic system, as pointed out in [9] a T^3 behavior is also expected, but a second energy gap temperature $T_{\rm AE2} > T_{\rm AE1} = T_{\rm AE}$ should occurs associated with the second hard axis. Since our calculation for $T_{\rm AE}$ is obtained from the phase diagram measured when H is applied along the easy axis this temperature corresponds to $T_{\rm AE1}$. However in the specific heat measured at $H = 0$ both temperature gap should play a role in the overall suppression of $C_{\rm m}$. Following the suggestion given by Lashley *et al* [12] for $T \leqslant T_{\rm N}/3$, $C_{\rm m}$ may be expressed by the empirical expression $C_{\rm m} = AT^n\, {\rm e}^{(-\Delta/T)}$, where n is either model calculated or empirically selected. If we choose that in this region ($\leqslant$2.2 K) n is set to $n = 3$, we obtain a gap $\Delta = 1.5$ K. This is larger than the gap obtained from the phase diagram, however as already pointed out the specific heat at $H = 0$ includes the effect of the different gaps present in the system and $T_{\rm AE1}$ is the smaller of those. The choice of $n = 2$ give a value $\Delta = 0.99$ K (inset of figure 7). This is close to the value obtained from the phase diagram but inconsistent with the T^3 behavior of $C_{\rm m}$ discussed above.

When the external field H is set along the easy axis the Joenk calculations [10] applies for $H_0 < H_{\rm SF}$, otherwise the sub-lattice will flop at $H_{\rm SF}$ to a direction perpendicular to the applied field. Below $H_{\rm SF}$, the degenerate spin wave modes are split by $\pm g\mu_{\rm B}H$. One set of modes has its gap raised the other lowered with increasing H. The overall effect due to the exponential dependence of the different branches of the gap is an increase of $C_{\rm m}$ with $H < H_{\rm SF}$. This was first discussed by Kouvell and Brooks [13] using a semi-classical approach to the free spin-wave treatment. Besides they also show that at the spin-flop transition, that occurs when the field is along the easy axis, a discontinuity in the specific heat $C_m(H)$ at $H_{\rm SF}$ is present and that $C_m(H)$ decreases with H in the SF phase. In our case only the feature related to the jump in the C at a fixed T at the spin-flop transition is retained, neither the steady increase of C in the AF region with the applied field nor the steady decrease of C in the SF phase are observed when H is along the easy axis. However, the qualitative features of the C versus H when H is applied perpendicular to easy axis coincides with the theoretical calculations of the Kouvell and Brooks report, namely an increase in C with field when approaching the transverse AF–P boundary and a peak in C with a subsequent decrease with H when entering the disordered paramagnetic phase, see for example figure 4(b) for $H_\perp$.

The calculation of Kouvel and Brooks [13] neglect the strong fluctuations associated with the lambda anomaly at the second order phase boundary. As already pointed out when we approach the phase boundary along an isotherm (figure 1(b)) C increases leading to the observed behavior in the C

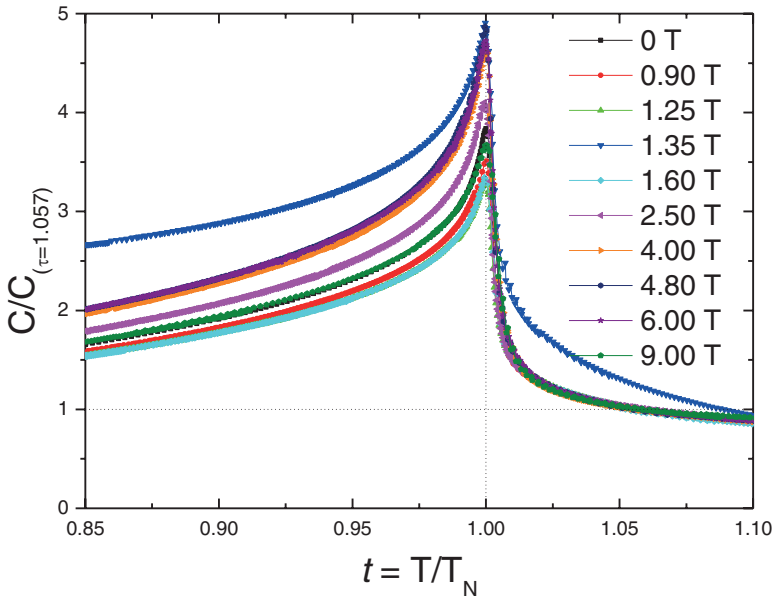

Figure 8. Specific heat for various fields normalized at $\tau = T/T_N(H) = 1.057$.

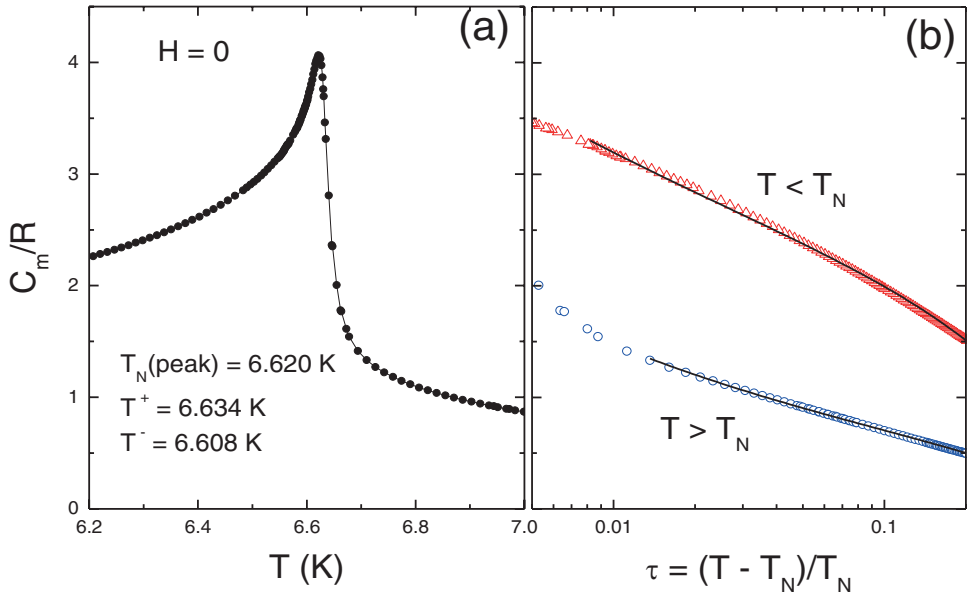

Figure 9. (a) C_m/R versus T in the region close to the T_N at $H = 0$. The fits were restricted to the region(s) below (above) the inflection points T^- (T^+). (b) Fitting regions in the log reduced temperature scale.

versus H curves. According to the critical analysis approach given by Riedel and Wegner [14] on approaching the phase boundaries either by varying the temperature or the field or even in a 'direction' involving a combinations of T and H the singularity should be of the same nature, this is an important result in the theory of critical phenomena. Thus the result we obtained is in accordance with the expected.

III.C. Critical behavior along the order–disorder boundaries to the paramagnetic phase

In this section we show that the behavior of the specific heat singularity in a reduced temperature scale $T/T_N(H)$, is preserved along the boundary. Figure 8 shows the specific heat for selected values of H covering the whole range of transitions to the paramagnetic phase, either from the AF or the SF phase. We made the choice to normalize C_m at a reduced temperature in the paramagnetic region in order to disclose the divergence in the high temperature side of the lambda transition. The close similarity between the curves obtained at $H = 0$ (marking the P–AF transition) and the curve at 9 T (P–SF transition) is remarkable. We will not attempt here to make a detailed analysis of the criticality in analyzing the values of the critical exponent α and the amplitude ratio (A^+/A^-), in the molds made in [15, 16] for MnF_2 and FeF_2, since this is not the main purpose of our paper. Instead we explore the internal consistency of the criticality along the boundaries to the disordered phase.

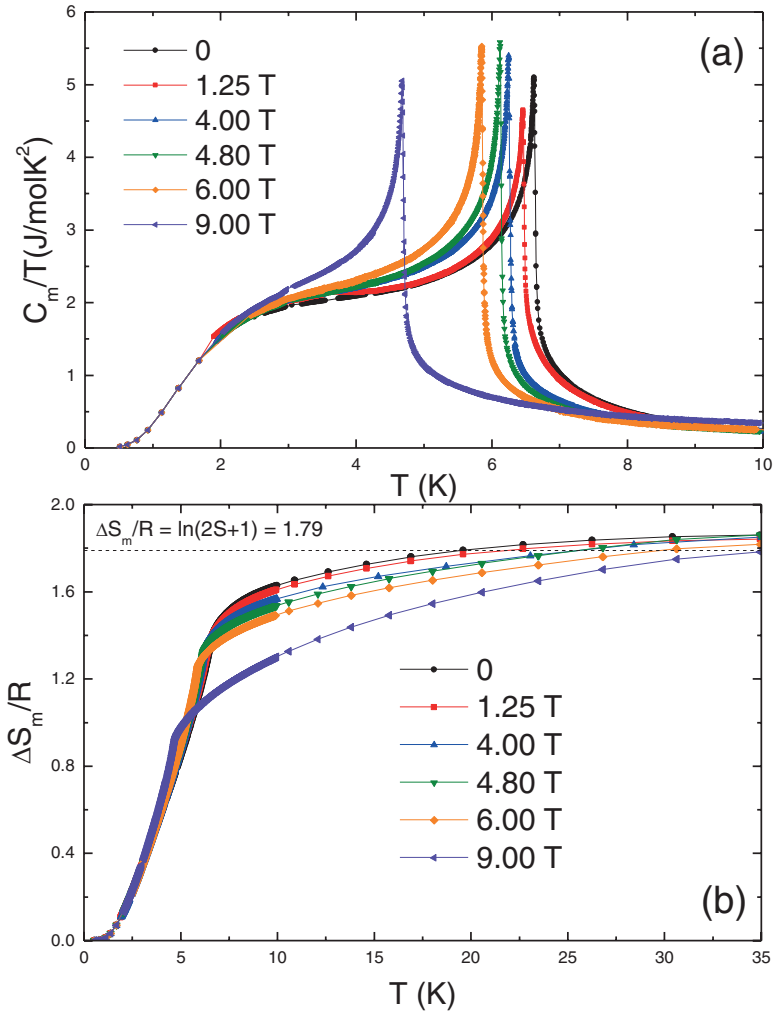

Figure 10. (a) Magnetic specific heat at various field values plotted as $C_{m,H}/T$ versus T and (b) the integrated entropy up to $T = 35$ K. In the paramagnetic region the effect of the applied field is to reduce the entropy due to the magnetic field alignment of the paramagnetic moments. About 80% of the total magnetic entropy reduction with T occurs below $T_N(H)$.

The data close to the divergence at $H = 0$ is shown in figure 9. The point where the rounding of the peak occurs will be excluded from our analysis and we will limit to temperatures above and below $\tau = (T - T_N)/T_N)$ in the interval $0.01 \leqslant |\tau| \leqslant 0.2$. The rounding cutoff taken from the inflection point in the curve are $T^+ = 6.634$ K and $T^- = 6.608$ K thus the actual T_N lies between those values. The data were fitted to the expression below for each side of the transition. We set $T_N = 6.62$ K in those fits:

$$C_m^{\pm} = (A^{\pm}/\alpha^{\pm})\,|\tau|^{-\alpha\pm} + b\tau$$

The two last terms contain the regular part of C_m. The unconstrained independent best fits gave respectively $A^- = 0.238 \pm 0.005$, $\alpha^- = 0.147 \pm 0.005$, $b^- = -2.8$ and $A^+ = 0.115 \pm 0.005$, $\alpha^+ = 0.278 \pm 0.005$, $b^+ = -0.8$. The ratio of the amplitudes (A^+/A^-), is close to the predicted theoretically for the Ising 3D model as also is the α^- exponent. The α^+ exponent in contrast is far off the theoretical prediction.

An analogous analysis was applied to the data obtained at 9 T when crossing the phase boundaries from the P phase to the SF phase. It gave respectively $A^- = 0.241 \pm 0.005$, $\alpha^- = 0.145 \pm 0.005$ and $b^- = -3.0$ and $A^+ = 0.114 \pm 0.005$, $\alpha^+ = 0.297 \pm 0.005$ and $b^+ = -0.62$. From this analysis we conclude that the critical behavior along the AF–P phase boundary (below the bicritical field) and the SF–P phase boundary (above the bicritical field) are basically the same. From the values obtained from ratio of the amplitudes (A^+/A^-), also from the α^- exponent this behavior is the expected for an Ising like character. Figure 9 is thus consistent with the fact that the number of critical component of the order parameter along the AF–P and SF–P phase boundaries is $n = 1$ (Ising like) on both branches of boundaries to the P phase.

If we make a similar comparison between the curves for C measured when H is parallel and perpendicular to the easy axis we can observe a similar temperature behavior for the lambda transition. This can be seen in figure 3(b) or in its normalized version C_m/T versus T/T_N (H) shown in figure 11 measured at the same applied field. Both curves in the AF phase are essentially identical pointing to a similar kind of critical behavior.

III.D. Magnetic contribution to the entropy

The entropy associated with the magnetic contribution at a given temperature T is given by

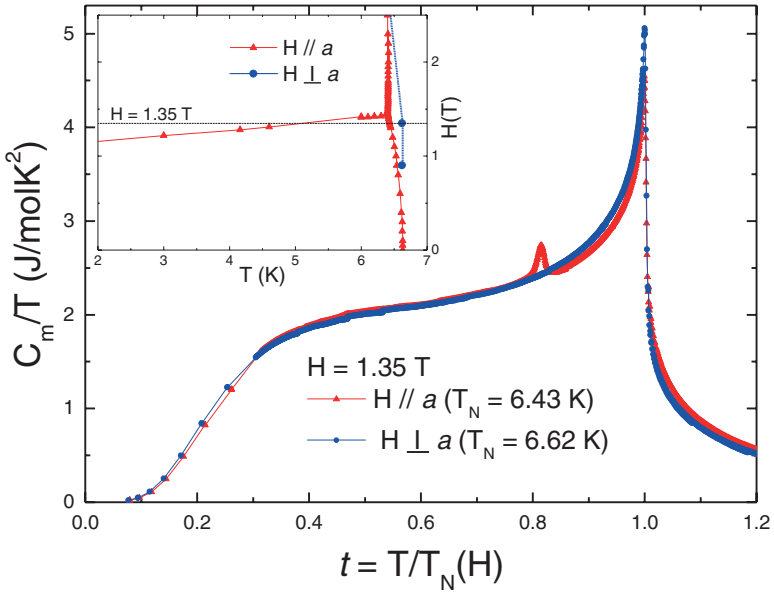

Figure 11. Magnetic specific heat divided by the temperature as a function of the reduced temperature $t = T/T_N$ measured at $H = 1.35$ T applied parallel and perpendicular to the easy a axis. The inset shows the phase diagram $H(T)$ for both magnetic field configurations.

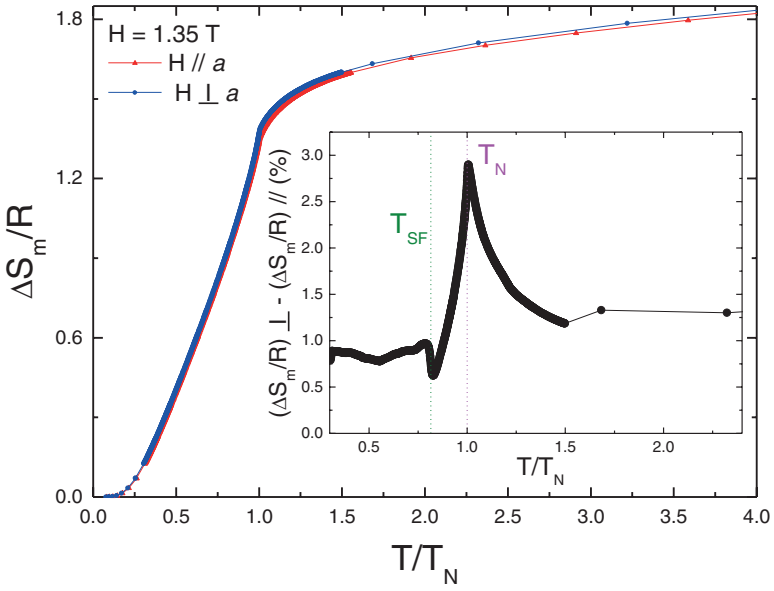

Figure 12. Integrated entropy for the parallel and perpendicular field configurations in a reduced temperature scale $t = T/T_N$. The inset shows the percentage difference of the entropy for both field configurations. The antiferromagnetic (T_N) and spin-flop (T_{SF}) transition temperatures are indicated.

$$S_{m,0}(T) = \int_0^T \frac{C_{m,0}}{T'} \mathrm{d}T',$$

where $C_{m,0}$ is the magnetic specific heat at zero applied field. If the magnetic field is not zero the subscripts (m, H) should be introduced in the above expression. The magnetic entropy change with the applied field is the difference $\Delta S_{m,H} = S_{m,H} - S_{m,0}$.

Figure 10(a) shows the specific heat as C_m/T versus T for different magnet fields and the correspondent integrated entropy is shown in figure 10(b). The entropy reduction occurs mostly in the ordered region, below $T_N(H)$, and it is of the order of 80% of the total entropy. In the paramagnetic region ΔS decrease with the applied field due to the partial alignment of the magnetic moments. In the ordered region the field effects on the entropy are less pronounced since the sub-lattice magnetization is almost field independent.

We can now focus on the change in entropy when the different magnetic phases under the two applied field configurations are considered. In figure 11 we compare the C_m/T curves measured at the same applied field (1.35 T) for H parallel and perpendicular to the easy a axis. This particular field value is very convenient because all phases are swiped in the temperature scan (see the inset of figure 11). Since at fields $H \neq 0$ the $T_{N//}(H)$ is always smaller than $T_{N\perp}(H)$ in order to perform a proper comparison we work with a reduced temperature

$t = T/T_N(H)_{//,\perp}$. We can see in figure 11 that the values of C_m/T are almost identical for both field configurations. After the passage to the AF phase, marked by the peak in C, which is related to the latent heat involved in this first order transition, the values of C_m/T is a slightly higher for the perpendicular field configuration. The higher value for C_m/T in the SF phase is consistent with the data measured along isotherms depicted in figure 4, where a jump towards a higher value of C_m occurs when the SF phase is entered from the AF phase at $H_{SF}(T)$. The area under the curves up to a temperature T is the entropy gain for the given field configuration as illustrated in figure 12. When the magnetic field is applied along to the easy axis the system is in the SF phase up to a reduced temperature $t = 0.8$ and in the AF phase between $0.8 < t < 1.0$. For the perpendicular configuration on the other hand, only the AF phase exist below $t = 1$. The inset in figure 12 shows that the percentage difference in entropy between the ordered phases in the two configurations is very small. In the ordered phases the integrated entropy for the perpendicular field configuration is larger due to the relative larger contribution of the SF phase up to 5.1 K. After the paramagnetic phase is entered the contribution from both field configurations is basically equal.

IV. Summary and conclusions

We conducted an experimental study of the behavior of the specific heat along the phase boundaries between the different magnetic phases in single crystals of $Cs_2FeCl_5{\cdot}H_2O$. We conclude that the transitions to the paramagnetic phase either when H is parallel or perpendicular to the easy axis have the same critical behavior, namely that they are 'Ising like' in nature. We also made a correlation with the observed magnetic AC susceptibility data and the thermal data when the first order phase boundary separating the AF and the SF phase is crossed either by varying the temperature or the magnetic field. The jump observed in C_m when the SF boundary is crossed by changing H, and the integration of the C_m/T curves for a given field applied parallel and perpendicular to the easy axis, for selected value of H in which the sweep in T spans over all phases present in the system, lead us to the conclusion that the SF phase has a lower entropy than the AF phase. Also either in the parallel or perpendicular field configuration the entropy in the AF phase is almost equal. The spin-wave analysis made on the data at $H = 0$ is consistent with the expected T^3 behavior for an antiferromagnet and with the presence of an energy gap in the spin-wave spectrum of the system that suppresses C_m at temperatures lower than $T_N/3$.

Acknowledgments

The authors would like to acknowledge support from the Brazilian agencies CNPq and FINEP.

References

[1] Carlin R L and Palacio F 1985 *Coord. Chem. Rev.* **65** 141
Paduan Filho A, Palacio F and Carlin R L 1978 *J. Physique Lett.* **39** L279
[2] Shapira Y and Foner S 1970 *Phys. Rev.* B **1** 3083
[3] Freitas R S, Paduan-Filho A and Becerra C C 2015 *J. Magn. Magn. Mater.* **374** 307
[4] Puértolas J A, Navarro R, Palacio F, Bartolomé J, González D and Carlin R L 1982 *Phys. Rev.* B **26** 395
[5] Greedan J E, Hewitt D C, Faggiani R and Brown I D 1980 *Acta Crystallogr. Sect.* B **36** 1927
[6] Campo J, Luzón J, Palacio F, McIntyre G J, Millán A and Wildes A R 2008 *Phys. Rev.* B **78** 054415
[7] Lashley J C *et al* 2003 *Cryogenics* **43** 369
[8] Kubo R 1953 *Rev. Mod. Phys.* **25** 344
[9] Eisele J A and Keffer F 1952 *Phys. Rev.* **96** 929
[10] Joenk R J 1962 *Phys. Rev.* **128** 1634
[11] Keffer F 1966 Spin waves *Handbuch der Physik* vol XVIII-2 ed H P J Wijn (*Ferromagnetism/Ferromagnetismus*) (Berlin: Springer) pp 108–16
[12] Lashley J C, Stevens R, Crawford M K, Boerio-Goates J, Woodfield B F, Qiu Y, Lynn J W, Goddard P A and Fisher R A 2008 *Phys. Rev.* B **78** 104406
[13] Kouvel J S and Brooks H 1954 *Technical Report No. 198* Cruft Laboratory, Harvard University
[14] Riedel E and Wegner F 1969 *Z. Phys.* **225** 195
[15] Nordblad P, Lundgren L, Figueroa E and Beckman O 1981 *J. Magn. Magn. Mater.* **23** 333
[16] Belanger D P, Nordblad P, King A R, Jaccarino V, Lundgren L and Beckman O 1983 *J. Magn. Magn. Mater.* **31** 1095